Anomalous Single-Frame Flux Uncertainties in WPHotpm

Document number: WSDC-D-T042

1. Overview of the Problem

During the integration and test period for WSDS v6, anomalously large flux uncertainties were observed to occur occasionally in the MEP (Multi-EPoch) output. This is a new product that gives greater visibility into stationary-fit single-frame flux solutions for sources being extracted by the multi-frame multi-band algorithm implemented in the WPHotpm program. An extreme case was observed in which a W3 flux uncertainty had the value of IEEE Inf (infinity). Other extremely large values were also found (e.g., in the billions of DN). These are believed to stem from the same mechanism as the Inf, since small changes in the way aperture photometry and background subtraction are done led to the replacement of the Inf with a value of 2123448.5. This makes it clear that the anomalous results stem from numerical instabilities in the matrix inversion that is part of the uncertainty calculation.

2 Review of the Stationary Model

The stationary fit solves for point-source fluxes and positions by applying the procedure described in the WPHOT SDS (WSDC D-D006), section 3.1.1. Sources are initially detected in multi-band co-added images in the MDET module and passed to WPHOT for extraction by fitting PSF templates to each frame in the co-add stack at each source position. The detections are processed in order of descending brightness, and as each is processed, nearby sources are identified and grouped into an ensemble of potentially blended sources. The source about which other sources are grouped is called the *primary component* of the ensemble. The idea is to include the entire ensemble in the fit in order to get the best estimates of the primary component's parameters; after that has been accomplished, the primary component is output, and all other components' solutions are discarded, since these sources will each come up later in the role of a primary component. Often the ensemble consists only of a primary component, particularly in regions of low source density. When a source is output, its flux-normalized PSF is subtracted from all frames in the stack.

To summarize the SDS, we have an observational model

$$\rho_{\lambda i} = b_{\lambda i} + \nu_{\lambda i} + \sum_{n=1}^{N_B} \left(f_{\lambda n} H_{\lambda} (\vec{r}_{\lambda i} - \vec{s}_n) \right)$$

where $\rho_{\lambda i}$ is the flux in the i^{th} usable observed pixel at the position given by the 2-vector $\vec{r}_{\lambda i}$ in the wavelength band λ, $\vec{s}_n$ is a 2-vector giving the position of the n^{th} blend component, $f_{\lambda n}$ is the flux of the n^{th} component, H_λ®) is the PSF, $b_{\lambda i}$ is the local background estimated in an annulus around pixel i, and $v_{\lambda i}$ is the noise in the i^{th} pixel, with prior noise variance $\sigma^2_{i\lambda}$, which includes uncertainty due to the PSF model based on an initial flux estimate from aperture photometry. For details on the computation of the background and noise, the definition of the chi-square goodness-of-fit statistic, and the algorithm for minimizing chi-square to obtain the solution, the reader is referred to the SDS.

The uncertainty estimates are obtained as follows. The Fisher information matrix G is computed, and the error covariance matrix γ expressing the parameter uncertainties is the inverse of G:

$$\ln P(\vec{\rho}|\vec{z},N_B) = -\frac{1}{2}\sum_\lambda \sum_i \left(\frac{\rho_{\lambda i} - b_{\lambda i} - \sum_{n=1}^{N_B} f_{\lambda n} H_\lambda(\vec{r}_{\lambda i} - \vec{s}_n)}{\sigma_{\lambda i}} \right)^2 + \text{const.}$$

$$G \equiv -\left\langle \frac{\partial}{\partial \vec{z}} \frac{\partial^T}{\partial \vec{z}} \ln P(\vec{\rho}|\vec{z},N_B) \right\rangle$$

$$\gamma = G^{-1}$$

$$\sigma(z_j)^2 = \gamma_{jj}$$

where $\vec{\rho}$ is the vector of all pixels used for the calculation, with N_{obs} elements, and $\vec{z}$ is the vector of all parameters being fit, with n_p elements. The G and γ matrices are therefore $n_p \times n_p$ in size. The components of the $\vec{z}$ vector are $[\{\vec{s}_n, (f_{\lambda n} : \lambda = 1 \text{ to } N_\lambda)\} : n = 1 \text{ to } N_B]$. For the complete multi-frame solution, N_{obs} is the total number of pixels available, and for single-frame solutions, it is the number of pixels for all bands in that single frameset.

These matrices are real and symmetric, as are all legitimate error covariance matrices and their inverses in practice. It can happen, however, that for some bands in some frames, the number of pixels available is less than the number of parameters being estimated, resulting in the matrices being singular. In some cases the matrices are nonsingular but contain too little information in a given band to yield a positive-definite error variance in that band. In such cases, the difficulties are encountered both in the parameter fit itself and in the error estimation, since in principle the same matrices are involved (but because of the nonlinearity of the problem and the chi-square minimization technique, the information appears in different forms). It has long been recognized that single-frame parameter fits frequently encounter matrix singularity, with the result that warning messages have been turned off, although a counter for the total number of such events is given in the processing summary. Typical values for a tile are on the order of 10^6.

If the G matrix is singular or if a diagonal element of γ is not positive definite, an attempt to estimate that diagonal element of γ is made by simply inverting the corresponding element of G. This requires the G element to be greater than zero. If this fixup cannot be done, the error covariance element is

returned as zero, which causes it to be set to null downstream in the processing.

3 A Case Study

The tile 0330p636_ac51-054137 exhibited the only case of an Inf uncertainty observed so far. Downstream processors now trap this value and null out the photometry for the offending frame, but anomalously large finite values are allowed to pass. The MEP data row on which the Inf occurred also contains the mdex position for the source, so it was possible to locate that source in the mdet list, obtain those coordinates, and use them to turn on “targeting debugging” inside WPHotpm (this is an extremely verbose mode for tracking all relevant details of a given source’s processing).

Since the mdex and mdet positions generally differ slightly and in some cases may differ by over 10 arcseconds, finding an mdex source in the mdet list is not always a trivial exercise. The mdet detection responsible for the anomaly turned out not to be the closest to the anomalous mdex source, missing by about 12 arcsec. The targeted debugging revealed that all the mdet detections in the vicinity were in three-component blend groups, one of which also produced an active deblend. The diagram below shows the mdet detections as blue dots connected to their red-dot mdex counterparts. The mdet detections are labeled by their target numbers and blend-group numbers, where the latter are numbered according to processing order, e.g., “b1" was the first blend group to appear. Note that the field is at high declination, so the true-angle RA scale is quite different from the Dec scale; the width in RA is 23.5 true arcsec, in Dec it is 36 arcsec.

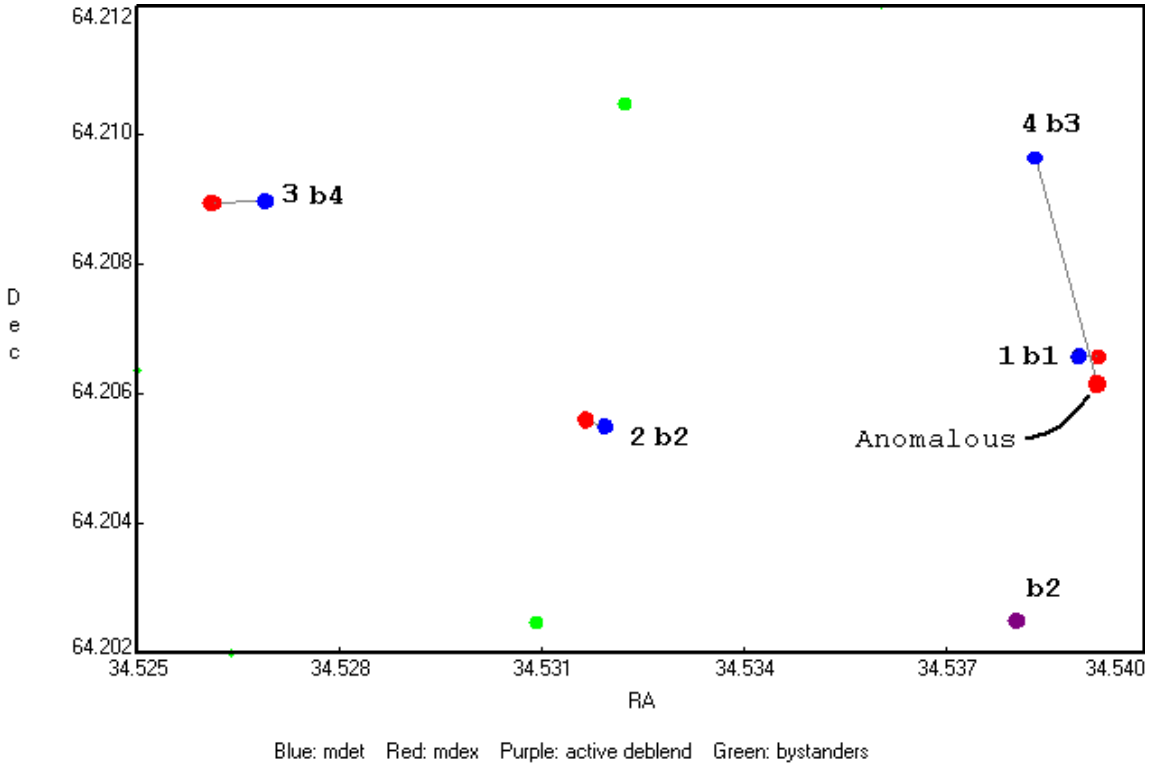

Target 1 was originally chosen because it is closest to the anomalous mdex source. The debug prints showed, however, that it did not produce that mdex source. It was in a blend group with two other sources (labeled 2 and 3 above), so those were added to the target list, but their debug prints also showed that neither of them was the culprit. Target 1 nevertheless probably plays a key role, because it is processed before any of the others, and therefore its flux is subtracted from the frames that eventually give rise to the anomalous source, which traveled 12.47 arcsec from its mdet position (labeled 4 above). The sequence of events was as follows.

Blend group b1 appears with targets 1, 2, and 3; targets 2 and 3 are dropped from the solution, and target 1 is output.

Blend group b2 appears for an untargeted source because it contains target 2 as a passive blend component along with another untargeted source; target 2 displaces the original primary component, and an active deblend is added to the mix; the original component is retained in the flux fitting, while the other passive-deblend component is dropped; target 2 is output as the blend-swapped main source, the active deblend (the purple dot above labeled as being in blend b2) is output, and the original primary component is postponed.

Blend group b3 appears with an untargeted primary component, an untargeted passive-blend component which is subsequently dropped from the flux solution, and target 4 as another passive-blend component; target 4 is blend-swapped as the new primary; the two sources cause the *G* matrix to be 12×12 (two position coordinates and four fluxes each); the fitting is done with pixels from which the flux of target 1 has been subtracted, and the fit is poor, requiring target 4 to migrate 12.47 arcsec from its mdet position to land just 1.43 arcsec from the mdex source for target 1; the single-frame fits involve mostly singular matrices, although the one that produced the anomalous W3 flux was not singular, but it appears to be very close (offline evaluation of its determinant at higher precision yielded zero) and numerically unstable.

Blend group b4 appears with target 3 as the primary and two passive-blend components, one of which is the one dropped from the flux solution for blend group b3; the processing is straightforward and has no impact on the anomaly.

Summary: processing blend group b1 set the stage by leaving flux-subtracted pixels behind for blend group b3 to deal with, and resulting numerical instabilities caused a large position shift for target 4 (but not enough to be diagnosed as a “runaway fit”) and very bad single-frame flux fits and uncertainty estimation. The frame where the anomalous W3 flux uncertainty occurred probably involved only tails of the PSF covering usable pixels; this is suggested by the very high flux for that frame, 1557297 DN, with an uncertainty of 2123448.5 DN and band-rchi2 (w3rchi2_ep) value of 83940.336.

There were 30 frames available for this source. The MEP records are shown below.

source_id_mf	src_mf	ra	dec	n_ep
0330p636_ac51-054141	54141	34.5392427	64.2061886	30
0330p636_ac51-054141	54141	34.5392427	64.2061886	30
0330p636_ac51-054141	54141	34.5392427	64.2061886	30
0330p636_ac51-054141	54141	34.5392427	64.2061886	30
0330p636_ac51-054141	54141	34.5392427	64.2061886	30
0330p636_ac51-054141	54141	34.5392427	64.2061886	30
0330p636_ac51-054141	54141	34.5392427	64.2061886	30
0330p636_ac51-054141	54141	34.5392427	64.2061886	30
0330p636_ac51-054141	54141	34.5392427	64.2061886	30
0330p636_ac51-054141	54141	34.5392427	64.2061886	30
0330p636_ac51-054141	54141	34.5392427	64.2061886	30
0330p636_ac51-054141	54141	34.5392427	64.2061886	30
0330p636_ac51-054141	54141	34.5392427	64.2061886	30
0330p636_ac51-054141	54141	34.5392427	64.2061886	30
0330p636_ac51-054141	54141	34.5392427	64.2061886	30
0330p636_ac51-054141	54141	34.5392427	64.2061886	30
0330p636_ac51-054141	54141	34.5392427	64.2061886	30
0330p636_ac51-054141	54141	34.5392427	64.2061886	30
0330p636_ac51-054141	54141	34.5392427	64.2061886	30
0330p636_ac51-054141	54141	34.5392427	64.2061886	30
0330p636_ac51-054141	54141	34.5392427	64.2061886	30
0330p636_ac51-054141	54141	34.5392427	64.2061886	30
0330p636_ac51-054141	54141	34.5392427	64.2061886	30
0330p636_ac51-054141	54141	34.5392427	64.2061886	30
0330p636_ac51-054141	54141	34.5392427	64.2061886	30
0330p636_ac51-054141	54141	34.5392427	64.2061886	30
0330p636_ac51-054141	54141	34.5392427	64.2061886	30

w1x_ep	w1y_ep	w1mpro_ep	w1sigmpro_ep	w1rchi2_ep	w1flux_ep	w1sigflux_ep
7.120	985.362	8.245	0.452	2729.643	79815.875	33205.035
1003.544	239.727	12.674	null	8.861	-680.697	675.070
880.274	161.942	12.454	0.454	4.268	1653.767	692.041
753.997	983.988	13.110	null	7.979	-376.134	451.703
758.228	69.502	11.277	0.181	6.144	4887.954	814.262
964.267	358.975	13.090	null	9.890	-1004.063	460.017
840.396	264.118	13.049	null	6.855	63.799	446.081
81.735	906.945	11.826	null	10.228	-1104.308	1474.882
9.392	71.914	11.809	null	6.424	253.711	1371.119
132.314	268.884	11.934	null	9.330	-831.973	1335.094
263.603	494.041	11.836	null	7.415	-164.005	1460.611
257.317	600.271	12.839	null	6.598	175.758	492.273
131.083	500.765	11.337	0.108	5.640	4627.976	460.947
340.830	821.276	11.324	0.085	5.738	4681.050	364.476
217.389	731.440	11.322	0.124	5.755	4689.723	536.917
95.510	630.921	11.529	0.153	4.528	3875.621	546.869
726.499	138.329	11.200	0.394	6.946	5248.097	1903.855
853.162	354.345	11.505	0.487	4.632	3964.211	1779.335
982.217	553.786	11.294	0.248	5.992	4812.655	1097.851
654.263	197.318	11.228	0.332	6.635	5114.710	1564.198
523.181	916.012	11.358	0.333	5.481	4538.455	1391.870
394.242	712.207	11.392	0.458	5.241	4395.957	1852.738
463.897	627.325	11.601	0.414	4.275	3628.128	1384.457
338.263	433.699	11.240	0.323	6.505	5056.693	1504.896
461.881	912.542	11.330	0.103	5.690	4655.316	440.191
585.552	90.980	11.470	0.101	4.797	4093.788	380.070
378.149	688.505	11.596	0.159	4.289	3643.188	534.522
509.774	768.355	11.075	0.103	8.667	5889.439	560.391
629.511	874.826	11.411	0.095	5.126	4322.462	378.500
716.388	190.826	11.371	0.097	5.383	4481.749	401.622

w2x_ep	w2y_ep	w2mpro_ep	w2sigmpro_ep	w2rchi2_ep	w2flux_ep	w2sigflux_ep
11.928	986.767	7.372	null	166.846	-9435.156	35491.527
999.146	236.881	12.824	null	5.441	-511.916	234.009
876.374	159.604	12.337	null	6.061	-640.427	366.696
754.548	982.321	12.720	null	3.787	-101.060	257.688
754.739	67.674	12.752	null	4.008	-164.302	250.142
960.650	356.293	12.742	null	6.129	-653.822	252.408
837.181	261.956	12.426	null	2.733	269.244	203.039
85.781	908.037	11.637	null	2.564	347.179	524.859
10.179	73.461	12.618	null	4.298	-242.315	282.918
133.341	269.873	12.103	null	4.135	-198.617	454.644
264.839	494.410	11.811	null	4.270	-234.800	594.924
259.072	600.651	12.703	null	3.288	56.700	233.347
133.152	501.724	11.621	0.165	2.094	1417.887	215.060
343.043	821.272	11.477	0.115	2.390	1618.098	171.955
219.938	731.971	11.487	0.150	2.366	1604.361	221.581
98.342	632.013	11.583	0.125	2.157	1468.009	168.429
723.482	136.652	11.073	0.363	4.493	2348.747	784.266
850.230	352.131	11.295	0.436	3.050	1914.834	769.672
979.348	551.024	11.698	0.386	1.994	1320.786	469.823
651.934	195.965	11.468	0.380	2.417	1633.021	571.400
524.709	915.268	11.161	0.261	3.814	2165.372	521.530
395.635	711.983	11.546	0.450	2.229	1519.683	629.367
464.515	626.805	11.409	0.350	2.595	1724.241	556.138
338.806	433.745	11.385	0.366	2.677	1761.938	594.256
463.785	912.047	11.609	0.145	2.114	1434.104	191.647
583.213	89.916	11.726	0.163	1.966	1286.632	192.968
379.570	688.351	11.706	0.213	1.986	1311.301	257.663
510.767	767.643	11.639	0.180	2.068	1394.411	230.624
630.279	873.628	12.019	0.290	1.869	982.381	262.200
713.657	189.199	11.701	0.128	1.991	1316.535	155.176

w3x_ep	w3y_ep	w3mpro_ep	w3sigmpro_ep	w3rchi2_ep	w3flux_ep	w3sigflux_ep
11.517	986.135	null	null	null	null	null
null	null	null	null	null	null	null
null	null	null	null	null	null	null
null	null	null	null	null	null	null
null	null	null	null	null	null	null
null	null	null	null	null	null	null
null	null	null	null	null	null	null
85.506	907.328	8.574	null	1.761	2691.440	1601.933
5.346	77.021	1.091	null	83940.336	1557297.000	2123448.500
130.108	271.838	8.581	null	1.762	2708.078	1573.043
263.527	494.696	8.927	null	1.862	1112.136	1573.219
null	null	null	null	null	null	null
null	null	null	null	null	null	null
null	null	null	null	null	null	null
null	null	null	null	null	null	null
null	null	null	null	null	null	null
722.949	136.691	7.937	0.155	3.886	10600.290	1510.197
851.611	350.464	8.558	null	1.770	2811.063	1586.259
982.604	547.753	9.115	null	1.968	406.397	1587.860
651.295	196.022	8.522	0.258	2.167	6183.967	1467.039
527.203	912.439	8.829	null	1.788	2088.653	1284.995
396.262	710.676	9.320	null	2.049	-49.547	1482.492
465.091	625.579	8.805	null	1.799	1934.322	1416.019
337.603	434.004	9.239	null	1.981	328.186	1433.120
null	null	null	null	null	null	null
null	null	null	null	null	null	null
null	null	null	null	null	null	null
null	null	null	null	null	null	null
null	null	null	null	null	null	null
null	null	null	null	null	null	null

w4x_ep	w4y_ep	w4mpro_ep	w4sigmpro_ep	w4rchi2_ep	w4flux_ep	w4sigflux_ep
3.299	490.344	3.019	null	467.866	4882.895	2469.719
null	null	null	null	null	null	null
null	null	null	null	null	null	null
null	null	null	null	null	null	null
null	null	null	null	null	null	null
null	null	null	null	null	null	null
null	null	null	null	null	null	null
40.639	451.526	7.425	null	1.511	48.323	60.712
4.804	38.659	6.204	null	1.722	130.163	196.278
66.087	135.987	7.820	null	1.516	-11.967	59.016
131.590	247.289	7.292	null	1.537	66.056	62.907
null	null	null	null	null	null	null
null	null	null	null	null	null	null
null	null	null	null	null	null	null
null	null	null	null	null	null	null
null	null	null	null	null	null	null
362.832	71.284	7.137	null	1.592	84.089	68.673
426.072	178.077	7.674	null	1.545	4.629	65.224
490.585	276.700	7.541	null	1.857	-115.021	76.282
326.749	100.480	7.373	null	1.557	51.721	63.185
261.252	455.990	7.802	null	1.555	-14.383	59.991
196.824	355.175	7.193	null	1.559	53.580	78.361
231.625	313.183	7.527	0.446	1.899	154.622	63.459
168.887	217.444	7.432	null	1.541	38.008	65.328
null	null	null	null	null	null	null
null	null	null	null	null	null	null
null	null	null	null	null	null	null
null	null	null	null	null	null	null
null	null	null	null	null	null	null
null	null	null	null	null	null	null

mjd	frame_id
55239.3238105	01806a225
55430.1263862	07576a043
55429.9940819	07572a054
55429.8619049	07568a055
55429.8617776	07568a054
55429.6633848	07561b079
55429.5310806	07557b079
55239.6546346	01817a201
55239.3236832	01806a224
55239.1913790	01802b224
55239.0590748	01798a224
55429.3326878	07552a055
55429.2003835	07548a055
55429.0019908	07541b080
55428.8696866	07537b080
55428.7373823	07533b080
55238.9928590	01797a200
55238.8605548	01793a200
55238.7282507	01789a200
55238.6620350	01786a224
55238.7944664	01790a225
55238.9267706	01794a224
55239.2575947	01805a200
55239.3898990	01809a200
55429.1342951	07545b080
55429.2664720	07549b079
55429.4649921	07556a055
55429.5972964	07560a055
55429.7296006	07564a055
55429.3987763	07553b079

The mdex information for the anomalous source is as follows.

```
|    source_id           |  src |   ra      |   dec     |sigra   |sigdec  |
 0330p636_ac51-054141      54141  34.5392427  64.2061886   0.2506   0.3114

|sigradec|  w1x   |  w1y   |   w2x  |  w2y   |  w3x   |
  -0.0570  326.735 3637.960  326.735 3637.960  326.735

|  w3y   |  w4x   |  w4y   |  w1sky  |w1sigsk|w1conf |
 3637.960  326.735 3637.960    17.866   3.373   0.000

|  w2sky  |w2sigsk|w2conf |  w3sky  |w3sigsk|w3conf |
    30.518   3.854   0.000  1710.778  28.420   0.000

|  w4sky  |w4sigsk|w4conf | w1snr| w2snr| w3snr|
   465.944  10.216   0.000    4.9    5.2    5.3

| w4snr|  w1flux   |  w1sigflux  |  w2flux   |  w2sigflux  |  w3flux   |
    1.5  2.6893E+03    5.5295E+02  1.0216E+03    1.9469E+02  3.1427E+03

|  w3sigflux  |  w4flux   |  w4sigflux  |w1mpro|w1sigmpro|   w1rchi2|
    5.9139E+02  3.4968E+01    2.3631E+01 11.926     0.223  2.093E+00

|w2mpro|w2sigmpro|   w2rchi2|w3mpro|w3sigmpro|   w3rchi2|
 11.977     0.207  1.512E+00  9.257     0.204  1.772E+00

|w4mpro|w4sigmpro|   w4rchi2|    rchi2 |nb |na |
  8.212      null  1.513E+00  1.764E+00   2   0

|w1frTr |w2frTr |w3frTr |w4frTr | w1Sat | w2Sat |
 0.00000 0.00000 0.00000 0.00000 0.00052 0.00000

| w3Sat | w4Sat |SatNum|w1mag |w1sigm|w1flg|
 0.00000 0.00314   0000 12.239  0.017     1

| w1Cov |w1mcor|w2mag |w2sigm|w2flg| w2Cov |
  31.978  0.261 12.231  0.024     1  31.724

|w2mcor|w3mag |w3sigm|w3flg| w3Cov |w3mcor|
  0.319 10.506  0.114     1  13.613  0.825

|w4mag |w4sigm|w4flg| w4Cov |w4mcor| w1mag_1 |
  7.999  0.287    17  13.987  0.576    12.950

| w1sigm_1|w1flg_1| w2mag_1 | w2sigm_1|w2flg_1| w3mag_1 |
     0.019       1    13.061     0.028       1    12.165

| w3sigm_1|w3flg_1| w4mag_1 | w4sigm_1|w4flg_1| w1mag_2 |
     0.177       1     9.672     0.531      17    12.500

| w1sigm_2|w1flg_2| w2mag_2 | w2sigm_2|w2flg_2| w3mag_2 |
     0.017       1    12.550     0.024       1    11.331

| w3sigm_2|w3flg_2| w4mag_2 | w4sigm_2|w4flg_2| w1mag_3 |
     0.114       1     8.575     0.287      17    12.276

| w1sigm_3|w1flg_3| w2mag_3 | w2sigm_3|w2flg_3| w3mag_3 |
     0.018       1    12.292     0.024       1    10.736

| w3sigm_3|w3flg_3| w4mag_3 | w4sigm_3|w4flg_3| w1mag_4 |
     0.085       1     7.814     0.195      17    12.134

| w1sigm_4|w1flg_4| w2mag_4 | w2sigm_4|w2flg_4| w3mag_4 |
     0.020       1    12.135     0.026       1    10.264
```

```
| w3sigm_4|w3flg_4| w4mag_4 | w4sigm_4|w4flg_4| w1mag_5 |
     0.069       1     7.286     0.157      17    12.034

| w1sigm_5|w1flg_5| w2mag_5 | w2sigm_5|w2flg_5| w3mag_5 |
     0.021       1    12.021     0.028       1     9.870

| w3sigm_5|w3flg_5| w4mag_5 | w4sigm_5|w4flg_5| w1mag_6 |
     0.058       1     6.903     0.140      17    11.947

| w1sigm_6|w1flg_6| w2mag_6 | w2sigm_6|w2flg_6| w3mag_6 |
     0.023      17    11.919     0.030       1     9.540

| w3sigm_6|w3flg_6| w4mag_6 | w4sigm_6|w4flg_6| w1mag_7 |
     0.051       1     6.609     0.132      17    11.842

| w1sigm_7|w1flg_7| w2mag_7 | w2sigm_7|w2flg_7| w3mag_7 |
     0.024      17    11.803     0.031       1     9.259

| w3sigm_7|w3flg_7| w4mag_7 | w4sigm_7|w4flg_7| w1mag_8 |
     0.045       1     6.364     0.128      17    11.689

| w1sigm_8|w1flg_8| w2mag_8 | w2sigm_8|w2flg_8| w3mag_8 |
     0.024      17    11.660     0.032       1     9.017

| w3sigm_8|w3flg_8| w4mag_8 | w4sigm_8|w4flg_8|w1NM  |
     0.042       1     6.161     0.127      17     15

|w1M  |w1magP |w1sigP1|w1sigP2|   w1k     |w1Ndf|
    27  11.695   0.684   0.132     0.80266    22

|w1mLQ|     w1mJDmin    |     w1mJDmax    |     w1mJDmean   |w2NM  |w2M  |
 60.28    55238.66203495    55430.12638616    55351.86279118     12    29

|w2magP |w2sigP1|w2sigP2|  w2k      |w2Ndf|w2mLQ|
  12.117   0.991   0.184     0.88060    20 16.43

|     w2mJDmin    |     w2mJDmax    |     w2mJDmean   |w3NM  |w3M  |w3magP |
    55238.66203495    55430.12638616    55350.67632349      2    11   9.735

|w3sigP1|w3sigP2|  w3k      |w3Ndf|w3mLQ|     w3mJDmin    |
   0.976   0.294     0.50206     9 11.27    55238.66203495

|     w3mJDmax    |     w3mJDmean   |w4NM  |w4M  |w4magP |w4sigP1|
    55239.65463457    55239.04704713      0    12   8.838   1.216

|w4sigP2|  w4k      |w4Ndf|w4mLQ|     w4mJDmin    |     w4mJDmax    |
   0.351     0.54967     8  0.09    55238.66203495    55239.65463457

|     w4mJDmean   |rho12|rho23|rho34| q12 | q23 |
    55239.07010014    80    36    10     5     0

| q34 |XSCprox|w1Rsemi| w1ba | w1pa |w1Gmag |
     0    null    null   null   null    null

|w1Gerr |w1Gflg|w2Rsemi| w2ba | w2pa |w2Gmag |
    null   null    null   null   null    null

|w2Gerr |w2Gflg|w3Rsemi| w3ba | w3pa |w3Gmag |
    null   null    null   null   null    null

|w3Gerr |w3Gflg|w4Rsemi| w4ba | w4pa |w4Gmag |
    null   null    null   null   null    null

|w4Gerr |w4Gflg|nIters|nSteps| MeanObsMJD |   ra_pm   |
    null   null     15    609 55248.155286  34.5402082
```

```
|   dec_pm  |sigra_pm|sigdec_pm|sigradec_pm|  PMRA   |  PMDec  |
  64.2029927   0.9657    0.6204      0.2965    0.1489    2.2635

| sigPMRA|sigPMDec|w1snr_pm|w2snr_pm|w3snr_pm|w4snr_pm|
   0.7867   0.3674      6.7      5.7      7.2      2.4

| w1flux_pm | w1sigflux_pm| w2flux_pm | w2sigflux_pm| w3flux_pm |w3sigflux_pm |
  4.3055E+04    6.4550E+03  1.6080E+04    2.8191E+03  1.1588E+05    1.6157E+04

| w4flux_pm | w4sigflux_pm|w1mpro_pm|w1sigmpro_pm|w1rchi2_pm|w2mpro_pm|
  3.9359E+02    1.6519E+02     8.915        0.163  3.402E+00     8.984

|w2sigmpro_pm|w2rchi2_pm|w3mpro_pm|w3sigmpro_pm|w3rchi2_pm|w4mpro_pm|
        0.190  2.098E+00     5.340        0.151  1.637E+00     6.512

|w4sigmpro_pm|w4rchi2_pm| rchi2_pm |pmcode|nIters_pm|nSteps_pm|
        0.456  1.524E+00  2.474E+00  3Y999         2        83
```

Last update - 29 July 2013

John W. Fowler - IPAC